

Modeling and Evaluation of Conduit Systems for Harmonics and Electromagnetic Fields

Volume 1

Prepared for

STEEL TUBE INSTITUTE OF NORTH AMERICA
2000 Ponce de Leon, Suite 600
Coral Gables, FL 33134
Phone: (305) 421-6326
email: STINA@steeltubeinstitute.org

Prepared by

A. P. Sakis Meliopoulos
E. Glytsis
Chien-Hsing Lee
School of Electrical and Computer Engineering
Georgia Institute of Technology
Atlanta, Georgia 30332

July 1997

Table of Contents

<i>Modeling and Evaluation of Conduit Systems for Harmonics and Electromagnetic Fields</i>	<i>1</i>
Executive Summary	1
1.0 Introduction	3
2.0 Technical Approach	4
3.0 Model Description	6
3.1 Modeling of Non-Conductive Conduit or Conductors in Free Air	6
3.2 Modeling of Conductive But Non-Magnetic Conduit-Encased System	7
3.3 Modeling of Magnetic Conduit-Encased Systems	9
4.0 Finite Difference Implementation	15
5.0 Laboratory Testing	18
6.0 Factors Affecting Magnetic Fields	37
7.0 Conclusions	41
Appendix A: Difference Equations at Boundary Points	42
Appendix B: Computer Generated Data, 25 Amperes, 60 Hz	44
Appendix C: Computer Generated Data, 50 Amperes, 60 Hz	45
Appendix D: Computer Generated Data, 25 Amperes, 190 Hz	46
Appendix E: Computer Generated Data, 50 Amperes, 190 Hz	47
Appendix F: Computer Generated Data, 25 Amperes, 310 Hz	48
Appendix G: Computer Generated Data, 50 Amperes, 310 Hz	49

Modeling and Evaluation of Conduit Systems for Harmonics and Electromagnetic Fields

Executive Summary

A computer model of conduit-encased power distribution systems has been developed. The model is capable of predicting the level of Electromagnetic Field density at any point around the system. The modeling capability includes Electrical Metallic Tubing (EMT), Intermediate Metal Conduit (IMC), Galvanized Rigid Conduit (GRC), Aluminum Conduit (ARC) and Non-Conductive (for example PVC) conduit.

The computer model has been validated with laboratory tests. The laboratory tests consisted of short runs of conduit-encased circuits which were energized with various levels of electric currents. The laboratory tests confirm the model prediction. The results of this work prove that Galvanized Rigid Conduit (GRC) is *most effective* in reducing electromagnetic field levels for an encased power distribution circuits. PVC coated Galvanized Rigid Conduit (GRC) is equally effective to non-coated GRC of same steel thickness. IMC and EMT also provide a substantial reduction in the electromagnetic field levels for encased power distribution circuits. The results also indicate that Aluminum conduit is *practically ineffective* in reducing low frequency electromagnetic fields. PVC or any other non-conductive plastic conduit is *totally ineffective* in reducing electromagnetic field levels for encased power distribution circuits.

Specific conclusions from the research program are:

1. PVC conduit does not affect electromagnetic fields from power circuits.
2. Aluminum conduit is *practically ineffective* in reducing electromagnetic fields at power frequency (60 Hz). Magnetic field reduction in aluminum conduit encased power systems is on the order of 10%. At higher frequencies the effectiveness of aluminum to shield against electromagnetic fields increases.

3. Steel conduit is *very effective* in reducing electromagnetic fields at power frequency (60 Hz). Magnetic field reduction in steel conduit encased power systems is on the order of 70% to 95%.
4. Non of the conduit provides shielding against the contribution to electromagnetic fields from ground currents.

Volume 1 is a summary report of the model, experimental results and comparisons.
Volume 2 includes the computer generated data.

This is Volume 1.

1.0 Introduction

The scope of this project was to develop a validated computer model which determines the conduit performance as a component of a power distribution system and computes the electromagnetic fields in and around the conduit. The model has been utilized to carry out a study of the performance of the conduit with respect to harmonics and electromagnetic fields. Specifically, the following were investigated (a) the effect of conduit in a power system with harmonics, (b) the effect of conduit on the electromagnetic field level around a conduit-encased power distribution system, and (c) the effect of buried conduit on the electromagnetic field level around a conduit-encased power distribution system. The performance of the steel conduit has been compared to the performance of Al conduit, PVC conduit and open wire systems.

2.0 Technical Approach

A computer model of a power distribution system with conduit-encased circuits has been developed. The model accounts for:

- (a) Harmonics.
- (b) Computation of electromagnetic fields anywhere in the vicinity of a conduit-encased power distribution system.
- (c) Conduit buried in soil.

In an actual installation, these systems may be in the vicinity of other metallic structures. Harmonics and electromagnetic field levels may be affected by these other structures. Analytical models typically limit their scope to well defined geometries of the circuits and conduits involved. It is a practical impossibility to try to model in detail all the extraneous structures near a power circuit. In view of these observations, the model focuses on power circuits encased in conduit suspended in air or buried in soil of uniform soil resistivity.

The general system which was modeled is illustrated in Figure 2.1. For harmonic analysis, the electric loads may be nonlinear and therefore they will be generators of harmonics. As a result, the electric current in the power conductors will be of the form:

$$i(t) = I_{m1} \cos (\omega t + \phi_1) + I_{m3} \cos (3\omega t + \phi_3) + \dots$$

The impedance of the conduit-encased power distribution system to the flow of current depicted in above formula and the interaction of the conduit system with the nonlinear load has been modeled and analyzed. It is important that the analysis considers multiple voltage transformations (as it is customary in industrial and commercial installations i.e. 12kV to 480 volts and then 480 Volts to 208 Volts). This issue has been addressed to determine interaction of harmonics from the two voltage levels.

A computational model for electromagnetic fields has been developed for the same system illustrated in Figure 2.1. The model is general in the sense that it provides (a) magnetic field density, and (b) magnetic field intensity at any user specified point. A user interface has been developed for the graphical display of magnetic field density and intensity in user specified areas.

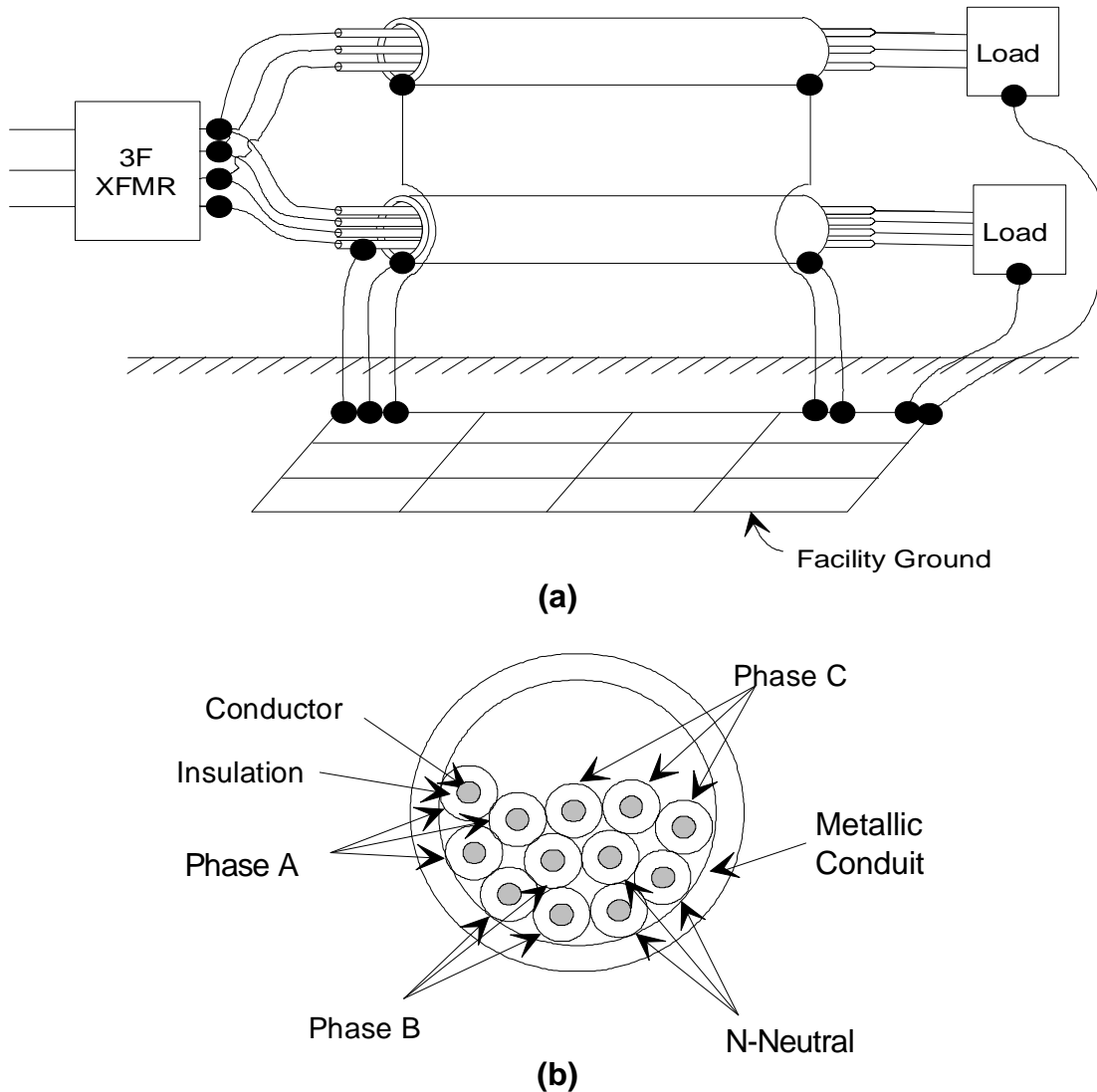


Figure 2.1. Conceptual Description of Conductive Conduit-Encased Secondary Distribution System

(a) Side View with Typical Grounding

(b) Cross Section of a Conductive Conduit-Encased Distribution Circuit

The model has been utilized for comparative studies. Specifically, the same analysis has been performed with the same system encased in steel conduit, aluminum conduit and PVC conduit. The results from these analyses have been compared to determine the relative effects of various conduit types. It was expected that the use of steel conduit would be beneficial in reducing harmonics and mitigating their propagation.

3.0 Model Description

The geometry of the analysis problem is shown in Figure 3.1. Non-magnetic (aluminum or copper) conductors are encased in a conduit (Conductive (magnetic or nonmagnetic) or non-conductive). The conductors may be placed in an eccentric position. The conduit inner and outer radii are a_{in} and a_{out} respectively. The analysis depends on the type of conduit used. In subsequent paragraphs we present the analysis method for three cases: (a) non-conductive conduit, (b) conductive but non-magnetic conduit and (c) magnetic conduit.

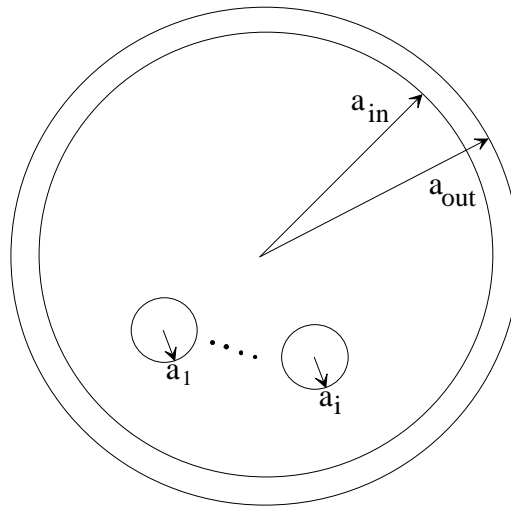


Figure 3.1. Illustration of Power Conductors Forming a Circuit and a Conduit

3.1 Modeling of Non-Conductive Conduit or Conductors in Free Air

This system does not include magnetic materials. Therefore the permeability of the system is that of the free space, i.e. the relative permeability is 1.0 everywhere:

$$\mu_r(H) = 1.0 \tag{1}$$

The power circuit may be encased in PVC conduit or suspended in air. From the analysis point of view, the PVC is ignored. As a result, the analysis of this circuit is limited to the power conductors. The solution method for this system is identical to the one described in

section 3.2 except that the conduit is not present. In the interest of avoiding duplication, the solution method for this system is not presented. The reader is referred to section 3.2.

3.2 Modeling of Conductive But Non-Magnetic Conduit-Encased System

This system also does not include magnetic materials. Therefore the permeability of the system is that of the free space, i.e. the relative permeability is 1.0 everywhere:

$$\mu_r(H) = 1.0 \quad (2)$$

The modeling procedure for this system is briefly described below. A single conduit with multiple conductors is illustrated in Figure 3.2 which also illustrates the modeling approach. Under balanced operating conditions, electric current will flow only in the phase conductors of the system. Most practical systems do not operate under balanced conditions and some electric current will flow in the conduit under normal operating conditions. The current distribution in the conductors and conduit obeys Maxwell's equations. For the purpose of deriving this current distribution, the cross section of the conductors and conduit is partitioned into *segments* as illustrated in Figure 3.2. For simplicity the figure shows the segmentation of only one cable inside the conduit. Because the cross section of a segment is small, the current distribution over the surface of a *segment* is assumed uniform. In this case, each *segment*, *i*, is characterized with a geometric mean radius, GMR_i , and a geometric mean distance, GMD_{ij} , from any other *segment*, *j*, in the system. These quantities are constant. The voltage across a *segment*, *i*, is given by the following equation:

$$\tilde{V}_i = \sum_j (r_{ij} + x_{ij}) \tilde{I}_j \quad (3)$$

$$\text{where } r_{ij} (\Omega / \text{m}) = \begin{cases} 0.9879 \times 10^{-6} f (\Omega / \text{m}) & j \neq i \\ \rho_i (T_i) \frac{1}{A_i} + 0.9879 \times 10^{-6} f (\Omega / \text{m}) & j = i \end{cases}$$

ρ_i is the resistivity of segment *i* material ($\Omega \cdot \text{m}$)

A_i is the cross section area of segment *i* (m^2)

T_i is the temperature of segment *i* ($^{\circ}\text{C}$)

$$x_{ij} = \frac{j\omega\mu_i}{2\pi} \ln \frac{D_e}{D_{ij}} \quad (4)$$

μ_i is the permeability of *segment* *i* material ($=\mu_0$)

$$D_{ij} = \begin{cases} GMD_{ij} & j \neq i \\ GMR_i & j = i \end{cases}$$

$$D_e = 2160 \sqrt{\frac{\rho}{f}} \times 0.3048 \text{ in meters}$$

ρ = soil resistivity in $\Omega \cdot \text{m}$

f = frequency of currents in Hz

$$\rho_i(T_i) = \rho_{i0} + \alpha_i (T_i - T_0) \quad (5)$$

α_i is a constant and T_i, T_0 in $^{\circ}\text{C}$.

Now assume that the first m_1 *segments* belong to conductor 1, the next m_2 *segments* belong to conductor 2, etc. and the last m_k *segments* belong to the magnetic conduit. Note that $k = N+1$ where N is the number of conductors. Writing one equation (3) for each segment in the above order one obtains the following equation in matrix form:

$$\begin{bmatrix} V^1 \\ V^2 \\ \vdots \\ V^k \end{bmatrix} = \begin{bmatrix} Z^{11} & Z^{12} & \dots & Z^{1k} \\ Z^{21} & Z^{22} & \dots & Z^{2k} \\ \vdots & \vdots & \ddots & \vdots \\ Z^{k1} & Z^{k2} & \dots & Z^{kk} \end{bmatrix} \begin{bmatrix} I^1 \\ I^2 \\ \vdots \\ I^k \end{bmatrix} \quad (6)$$

where

V^1 is a vector of voltages across *segments* of conductor 1 (an $m_1 \times 1$ vector).

I^1 is a vector of currents flowing through the *segments* of conductor 1 (an $m_1 \times 1$ vector), etc.

$k = N + 1$.

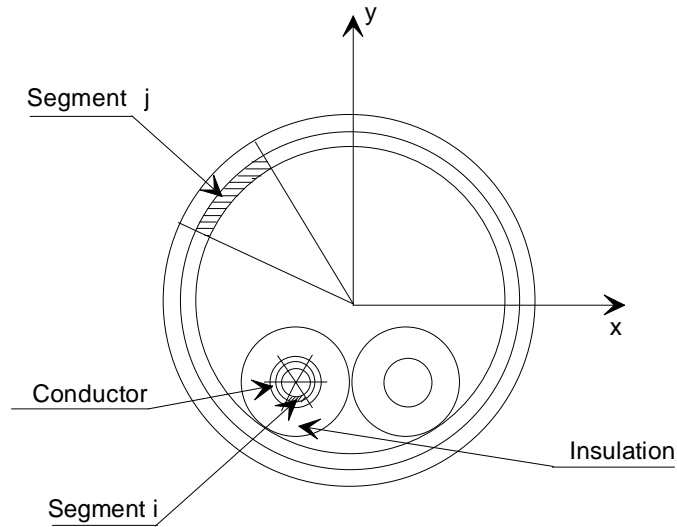


Figure 3.2. Illustration of Partitioning the Conductive Parts of a Magnetic Conduit Enclosed Power System into Segments.

Note that the sum of elements in vector I^1 is the total current I_1 through conductor 1, etc. Also note that the voltages in the vector V^1 must be the same and equal to V_1 , the voltage along conductor 1, since there is no voltage drop along the cross section of a conductor (otherwise current will flow perpendicular to the conductor). Equation (6) is inverted and subsequently the first m_1 equations are summed yielding one equation, the next m_2 equations are summed yielding another equation, etc. The final result is $k = N+1$ equations

where the total current through the conductors and the magnetic conduit appear, i.e.

$$\begin{bmatrix} \tilde{I}_1 \\ \tilde{I}_2 \\ \vdots \\ \tilde{I}_k \end{bmatrix} = \begin{bmatrix} y_{11} & y_{12} & \cdots & y_{1k} \\ y_{21} & y_{22} & \cdots & y_{2k} \\ \vdots & \vdots & \ddots & \vdots \\ y_{k1} & y_{k2} & \cdots & y_{kk} \end{bmatrix} \begin{bmatrix} \tilde{V}_1 \\ \tilde{V}_2 \\ \vdots \\ \tilde{V}_k \end{bmatrix} \quad (7)$$

The above equation represents the model of N power conductors enclosed in magnetic conduit. This model provides the electric current flowing into the power conductors and the magnetic conduit for a given set of applied voltages. This model is directly used in a nodal analysis for the entire system providing the voltages $\tilde{V}_1, \tilde{V}_2, \dots$. Once the voltages are known, the current distribution is computed from Equation (6). It is important to note that the current density, J, in a segment i can be computed by dividing the current in segment i by the cross area of the segment i.

Note that the solution for nonmagnetic conduit is direct, that is no iterations are involved.

3.3 Modeling of Magnetic Conduit-Encased Systems

The geometry of this problem is identical to that of section 3.2. The only difference is that the conduit is magnetic. The magnetic properties of the conduit are described through the magnetic field dependent relative permeability $\mu_r(H)$ given by

$$\mu_r(H) = \begin{cases} \frac{B_0}{\mu_0} \frac{H^{\alpha-1}}{H_0^\alpha} & (H \geq H_0) \\ \mu_{r,\max} & (H \leq H_0) \end{cases} \quad (8)$$

$$\mu_r(H) = 1.0 \quad (9)$$

Where H and B are the total magnetic field amplitude and total magnetic flux density amplitude respectively in the magnetic material, μ_0 is the free space permeability, and $B_0, H_0, \alpha,$ and $\mu_{r,\max}$ are material dependent parameters. Equation (8) applies to magnetic conduit and equation (9) applies to the remaining part of the system, i.e. the power conductors, the insulation and the air.

For the magnetic conduit calculations presented in this report the parameters of the model were: $B_0 = 0.5T$, $H_0 = 306A / m$, $\alpha = 0.125$, and $\mu_{r,max} = 1300$.

The magnetic field analysis problem is inherently nonlinear due to the presence of the magnetic conduit. In this project a quasi-static (for low frequencies as well as the 60 Hz of the power system) approach was followed [S. R. H. Hoole, *Computer-Aided Analysis and Design of Electromagnetic Devices*, Elsevier Science Publishing Company, New York 1989]. The magnetic field \vec{H} (vector variable) in every region is written as a sum of two terms:

$$\vec{H} = \vec{H}_c + \vec{H}_m \quad (10)$$

where the first term, \vec{H}_c , is the magnetic field that results from assuming that everything in the system remains identical to the original problem except that the conduit material is non-magnetic (non-permeable). The second term, \vec{H}_m , expresses the perturbation of the magnetic field due to the presence of the magnetic material in the conduit region. Using this approach, the original problem is broken down into two sub-problems. The first sub-problem involves the solution of the magnetic field problem in the case of a system of non-magnetic conductors and conduit. The first sub-problem is identical to the problem described in section 3.2 and it is not repeated here again. Note that the solution described in section 3.2 provides the current density distribution in the cross section of the power conductors and the conduit.

The term \vec{H}_c satisfies the following Maxwell's equation:

$$\nabla \times \vec{H}_c = \vec{J} \quad (11)$$

where the radiation term (displacement current has been dropped due to the quasi-static approximation). The term \vec{J} denotes the current density which is determined from the solution of the first sub-problem along with the calculation of \vec{H}_c . Since the total magnetic field \vec{H} also satisfies Equation (11) it can be deduced that \vec{H}_m satisfies the homogeneous curl equation $\nabla \times \vec{H}_m = 0$ and consequently it can be expressed as the gradient of a scalar magnetic potential function Φ :

$$\vec{H}_m = -\nabla\Phi \quad (12)$$

It follows that the divergence of the total magnetic potential Φ satisfies the following equation:

$$\nabla \cdot (\mu \nabla \Phi) = \nabla \cdot (\mu \vec{H}_c) \quad (13)$$

In above equation \vec{H}_c is known from the solution of the first sub-problem (the non-magnetic materials sub-problem). For a region of constant relative permeability the above equation is written in the form

$$\mathbf{m} \nabla^2 \Phi = \mathbf{m} \nabla \cdot \vec{H}_c = 0 \quad (14)$$

since the \vec{H}_c magnetic field has also a zero divergence. The last equation is a Laplace equation for the scalar magnetic potential Φ . Equation (14) needs to be solved for each region of the second sub-problem which is depicted in Figure 3.2. Since there is a magnetic material (steel conduit), the scalar magnetic potential must satisfy a boundary condition at the boundaries between materials of differing relative permeability ($r = a_{in}$ and $r = a_{out}$ in Figure 3.1). At these boundaries the normal component of the total magnetic flux density must be continuous. If $r = r_b$ represents the boundary surface between two media of permeabilities μ_1 and μ_2 , then the following conditions must be satisfied:

$$\Phi_1(r = r_b) = \Phi_2(r = r_b) \quad (15)$$

$$\begin{aligned} \mu_1 H_{r1}(r = r_b) &= \mu_2 H_{r2}(r = r_b) \\ \text{or} \quad \mu_1 [H_{cr1} - \frac{\partial \Phi_1}{\partial r} |_{r_b}] &= \mu_2 [H_{cr2} - \frac{\partial \Phi_2}{\partial r} |_{r_b}] \end{aligned} \quad (16)$$

where H_{ri} , H_{cri} , and Φ_i ($i=1, 2$) are the radial component of the total magnetic field, the radial component of \vec{H}_c (first sub-problem), and the scalar magnetic potential, respectively. However, the solution of the first sub-problem \vec{H}_c must satisfy the condition $H_{r1}(r = r_b) = H_{r2}(r = r_b) = H_{cr}(r = r_b)$ (continuity of normal H_c component). Using the last equality the second boundary condition is written as

$$\mu_1 \frac{\partial \Phi_1}{\partial r} |_{r_b} = \mu_2 \frac{\partial \Phi_2}{\partial r} |_{r_b} - (\mu_2 - \mu_1) H_{cr}(r = r_b) \quad (17)$$

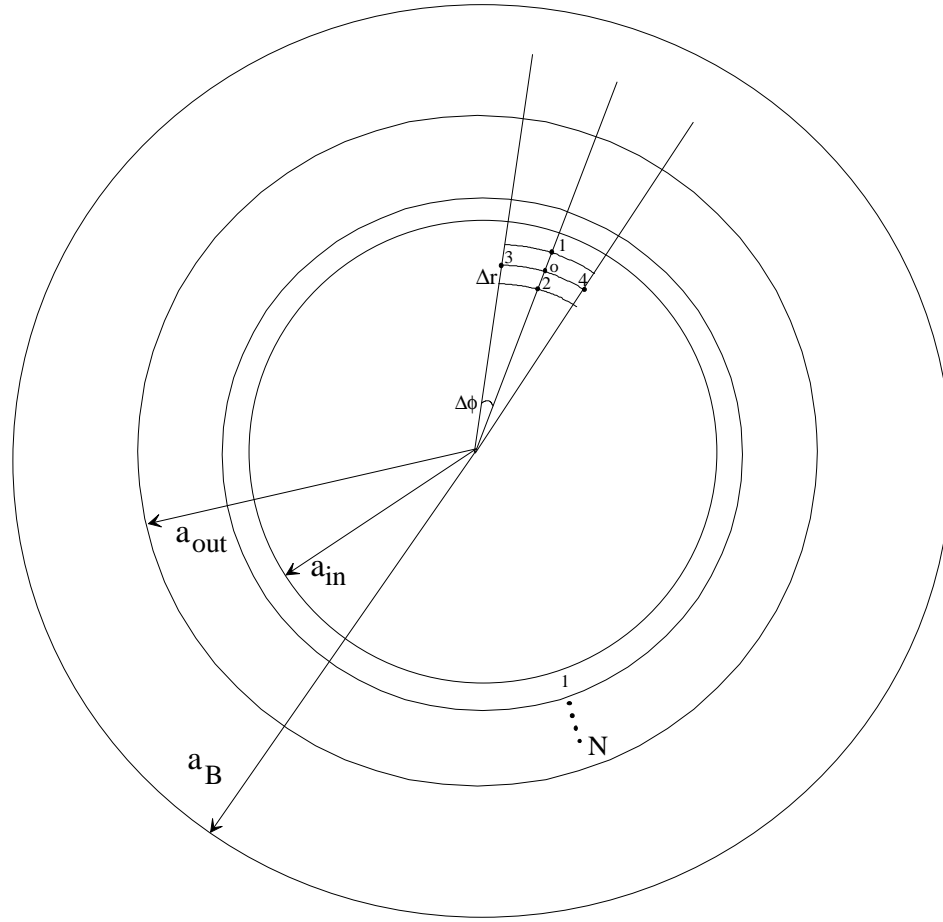


Figure 3.3. Illustration of Conduit Segmentation into Slices

The last equation contains the term H_{cr} ($r = r_b$) which in general will have angular dependence since the non-magnetic conductors are eccentric. This term forces the scalar magnetic potential to also be an angular dependent quantity. Therefore for any region in which Equation (14) needs to be solved the scalar magnetic potential will have both radial and angular dependence i.e. $\Phi = \Phi(r, \mathbf{f})$ (assuming a cylindrical coordinate system) and Equation (14) reduces to

$$\frac{\nabla^2 \Phi}{r^2} + \frac{1}{r} \frac{\nabla \Phi}{\nabla r} + \frac{1}{r^2} \frac{\nabla^2 \Phi}{\nabla \mathbf{f}^2} = 0 \quad (18)$$

The resulting magnetic field \vec{H}_m is given by

$$\vec{H}_m = -\frac{\mathcal{H}\Phi}{\mathcal{H}r} \hat{r} - \frac{1}{r} \frac{\mathcal{H}\Phi}{\mathcal{H}} \hat{f} \quad (19)$$

where \hat{r} and \hat{f} are the unit radial and tangential vectors at point (r, \mathbf{f}) . Equations (18) and (19) cannot be solved analytically due to the angular and radial dependence of the scalar magnetic potential. These equations are solved using the finite-difference technique. The discretized equations and their corresponding boundary conditions are summarized in section 4.0.

Equation (18) also needs to be solved in the region outside the conduit. This region is unbounded. Since Equation (18) is solved numerically, an artificial boundary is used sufficiently far from the conduit at a distance $r = a_B$ (see Figure 3.3). At this artificial boundary a suitable boundary condition is used. There are two possible choices. The first one is to set the scalar magnetic potential at $r = a_B$ to zero since this potential tends to zero as $r \rightarrow \infty$. The second condition is to set the radial (normal) derivative of the magnetic scalar potential to zero. This is justified since at a sufficiently large distance away from the conduit-and-conductors system, the magnetic field will have a tangential component only. The latter is the boundary condition used in this analysis.

The above analysis is applied to all segments of the conduit (the segmentation of the conduit is illustrated in Figures 3.2 and 3.3). Specifically, the conduit is divided into a number (N in Figure 3.3) of concentric layers (rings) and the relative permeability of each layer is known and assumed to be constant within the layer. Then, Equation (18) is solved within each region under the boundary conditions described by Equations (15) and (16). After the calculation of the scalar magnetic potential the total magnetic field is computed everywhere. Consequently, a new estimate of the relative permeability profile of the conduit is computed. Then the procedure is repeated until the relative permeability profile of the conduit and the resulting total magnetic field are self-consistent, i.e. they satisfy Maxwell's equations.

In summary, the algorithmic steps of the solution are:

1. Calculation of the magnetic field \vec{H}_c that results from the solution of the non-magnetic problem (first sub-problem, Figure 3.2).
2. Separation of the conduit in N concentric layers with relative permeabilities specified from Equation (1) where $\mathbf{H} = |\vec{H}_c|$.
3. Solution of the Laplace Equation (10) for each region of the second sub-problem (Figure 3.2) under the boundary conditions (7) and (9).

4. Calculation of the perturbation magnetic field \vec{H}_m from Equation (11).
5. Calculation of the total magnetic from Equation (2).
6. Repetition of step 2 with relative permeabilities computed using the total magnetic field computed in step 5.
7. Repetition of step 2 through 6 until a self-consistent magnetic field profile and relative permeability profile are obtained.

4.0 Finite Difference Implementation

The Laplace's equation for the scalar magnetic potential Φ [Equation (10)] is discretized using a cylindrical two-dimensional grid as shown in Figure A.1. It is assumed that within a region in which the Laplace's equation is solved the radial, Δr , and angular, $\Delta\phi$, grid spacings are constant. Considering the points 0 through 4 in Figure 3.2 we derive the difference equation corresponding to Equation (10):

$$\frac{\Phi_1 - 2\Phi_0 + \Phi_2}{(\Delta r)^2} + \frac{1}{r^0} \frac{\Phi_1 - \Phi_2}{2\Delta r} + \frac{\Phi_3 - 2\Phi_0 + \Phi_4}{(r_0\Delta\phi)^2} = 0 \quad (12)$$

which is also written as

$$2\left[1 + \left(\frac{\Delta r}{r_0\Delta\phi}\right)^2\right]\Phi_0 = \left[1 + \frac{\Delta r}{2r_0}\right]\Phi_1 + \left[1 - \frac{\Delta r}{2r_0}\right]\Phi_2 + \left(\frac{\Delta r}{r_0\Delta\phi}\right)^2\Phi_3 + \left(\frac{\Delta r}{r_0\Delta\phi}\right)^2\Phi_4 \quad (13)$$

Φ_i ($i = 0, 1, \dots, 4$) is the scalar potential at grid points 0 through 4 respectively and r_0 is the radial coordinate of point 0. Equations (12) or (13) are written for any point within a homogeneous region in the grid.

Of particular interest are the points that lie at the boundary between two regions of differing permeability. In this case the boundary condition expressed by Equation (9) is written in a discretized form. The continuity of the scalar potential across a boundary is accomplished by using grid points exactly at the boundary surface between the different regions. In order to achieve the latter it is imperative to use unequal radial grid spacing from region to region. Assuming that S is the boundary between two regions 1 and 2 of permeabilities μ_1 and μ_2 (as shown in Figure A.1) the radial grid spacings are Δr_1 and Δr_2 respectively. It is noted that it is not necessary to have unequal angular grid spacing for this problem. It is shown in Appendix A that the discretized form of Equation (9) is given by the following expression:

$$\left[2 \frac{\Delta r_2}{\Delta r_1} \frac{\mu_1 \left(1 - \frac{\Delta r_2}{2r_0}\right) + \mu_2 \left(1 + \frac{\Delta r_1}{2r_0}\right) \frac{\Delta r_1}{\Delta r_2}}{\mu_1 \left(1 - \frac{\Delta r_2}{2r_0}\right) + \mu_2 \left(1 + \frac{\Delta r_1}{2r_0}\right) \frac{\Delta r_2}{\Delta r_1}} + 2 \frac{\Delta r_1 \Delta r_2}{r_0^2 \Delta\phi^2} \right] \Phi_0 =$$

$$\begin{aligned}
& \frac{2\mu_2(1 + \frac{\Delta r_1}{2r_0})}{\mu_1(1 - \frac{\Delta r_2}{2r_0}) + \mu_2(1 + \frac{\Delta r_1}{2r_0}) \frac{\Delta r_2}{\Delta r_1}} \Phi_1 + \frac{2\mu_1(1 - \frac{\Delta r_2}{2r_0})}{\mu_1(1 - \frac{\Delta r_2}{2r_0}) + \mu_2(1 + \frac{\Delta r_1}{2r_0}) \frac{\Delta r_2}{\Delta r_1}} \Phi_2 \\
& + \frac{\Delta r_1 \Delta r_2}{r_0^2 \Delta \phi^2} (\Phi_3 + \Phi_4) - \frac{\Delta r_2}{2} \frac{4(\mu_2 - \mu_1)(1 + \frac{\Delta r_1}{2r_0})(1 - \frac{\Delta r_2}{2r_0})}{\mu_1(1 - \frac{\Delta r_2}{2r_0}) + \mu_2(1 + \frac{\Delta r_1}{2r_0}) \frac{\Delta r_2}{\Delta r_1}} H_{cr0}
\end{aligned} \tag{14}$$

Note that equation (14) reduces to Equation (13) in the case of a homogeneous region when $\mu_1 = \mu_2$ and $\Delta r_1 = \Delta r_2 = \Delta r$.

The outer artificial boundary at $r = a_B$ needs to be treated as follows. The points on this boundary satisfy the condition $\partial \Phi / \partial r = 0$. Using the approach described in Appendix A it is shown that each point in the artificial boundary satisfies the following discretized boundary condition:

$$\left(2 + 2 \frac{\Delta r^2}{r_0^2 \Delta \phi^2}\right) \Phi_0 = 2\Phi_2 + \frac{\Delta r^2}{r_0^2 \Delta \phi^2} (\Phi_3 + \Phi_4) \tag{15}$$

Finally, the origin of cylindrical coordinate system satisfies the condition

$$\Phi_0 = \frac{1}{N} \sum_{i=1}^N \Phi_i \tag{16}$$

where Φ_i ($i = 1, 2, \dots, N$) are the closest neighbor to the origin points.

Equation (13) or (14) or (15) or (16) are written for each grid point of the problem defined in Figure 3.2 (second subproblem). These equations form a set of linear equations which can be written in the following compact matrix notation.

$$[A][\Phi] = [b] \tag{17}$$

where $[A]$ is a coefficient matrix of dimensions $m \times m$ (where m is the total number of grid points), $[\Phi]$ is a vector of length m containing the scalar magnetic potential of the grid points, and $[b]$ is the source vector of length m the nonzero terms of which are due to the boundary condition (9).

The solution of the system of equations (17) specifies the scalar magnetic potential at each grid point. Then, the \vec{H}_m can be found using the discretized form of equation (11). Using an equation analogous to Equation (A7) and the Taylor expansions (A2) and (A3) the following is obtained after a lengthy but straightforward procedure:

$$\begin{aligned} \vec{H}_m|_0 = & -\frac{\partial\Phi}{\partial r}\Big|_0 \hat{r}_0 - \frac{\partial\Phi}{\partial\phi}\Big|_0 \hat{\phi}_0 - \frac{\Phi_4 - \Phi_3}{2\Delta\phi} \hat{\phi}_0 \\ & - \left(\frac{2}{\Delta r} + \frac{1}{r_0}\right)^{-1} \left[\frac{2}{\Delta r^2} (\Phi_0 - \Phi_2) - \frac{1}{r_0^2 \Delta\phi^2} (\Phi_3 + \Phi_4 - 2\Phi_0) \right] \hat{r}_0 \end{aligned} \quad (18)$$

where $\hat{r}_0 = \hat{x} \cos\phi_0 + \hat{y} \sin\phi_0$ and $\hat{\phi}_0 = -\hat{x} \sin\phi_0 + \hat{y} \cos\phi_0$ (hatted variables denote unit vectors).

5.0 Laboratory Testing

A series of laboratory tests were conducted to measure the magnetic fields near the conduit-encased power systems. It was validated that non-conductive conduit has no effect on magnetic fields and therefore no further testing was necessary for this conduit. The validation consisted of measuring the magnetic field with and without the non-conductive conduit. Seventeen samples of various steel and aluminum conduit and copper conductors were assembled. The description of the samples used is given in Table 5.1. For each sample two experimental setups were used. These are illustrated in Figures 5.1 and 5.2. Figure 5.1 illustrates the setup used for energizing the system with 60 Hz currents. For this set of experiments, two levels of energization were used: (a) 25 Amperes, 60 Hz and (b) 50 Amperes, 60 Hz. Figure 5.2 illustrates the setup used to energize the system with harmonics. Specifically, an audio amplifier was used to amplify a signal generated from an arbitrary function generator. This generator is capable of generating any waveform desired. In this report we present measurement data of harmonics, specifically near the third and fifth harmonics (190 Hz and 310 Hz).

The magnetic field meter is a three axes meter. Measurements were obtained at four different distances from the axis of the conduit or the axis of the circuit for each sample tested. Measurements of magnetic field near a power circuit may vary because of two factors: (a) the meter has finite dimensions and (b) the position of conductors inside the conduit make the magnetic field polarized and directional, i.e. different magnitude at different directions. For example, the magnetic field density varies as the probe moves around the conduit while the distance to the conduit axis is maintained constant. Also, the magnetic field density may vary if the meter is rotated in such a way that its center is stationary, even if it is a three-axes meter. To minimize the variability from these factors, the measurement consisted of the maximum and minimum magnetic field density of all measurements obtained at the same distance from the conduit axis. Specifically, the measurements were performed as follows: A 3-Axis ELF Magnetic Field Meter was used to measure the magnetic field density at 4 distinct points equidistant from the conduit axis. A calibrating string was used to maintain the constant distance for each measurement point. Four measurements were recorded for each of the four designated points around the conduit. Each set of values was averaged, and the minimum and maximum of the four average values were used to calculate the reduction of magnetic field. The minimum and maximum values are reported in this document.

Table 5.2 illustrates the measured data when the system is energized with 25 Amperes, 60 Hz. Table 5.3 illustrates measurements of magnetic field density around an aerial set of conductors, carrying 25 Amperes. Table 5.4 illustrates the measured data when the system is energized with 50 Amperes and Table 5.5 illustrates measurements of magnetic field density around an aerial set of conductors carrying 50 Amperes. Note that the measurements are performed at distances comparable to those around the conduits. The reduction of the magnetic field in percent, because of the presence of the conduit, can be computed by taking the ratio of two comparable measurements.

$$\text{Reduction of Magnetic Field (in percent)} = \left(1.0 - \frac{B_c}{B_{air}} \right) 100$$

where: B_c is the magnetic field density for the conduit-encased system, and B_{air} is the magnetic field density for the power circuit without conduit at the same point and for PVC conduit at the same point.

The actual reduction of magnetic field in percent has been calculated using equation (19) and reported in Table 5.6, column 1 for the 25 Ampere current level and in column 3 for the 50 Ampere current level. The same measurements have been repeated for the 50 Amperes current level. The measured values are reported in tables 5.4 and 5.5. The measured reductions of magnetic field in percent are listed in Table 5.6, column 3.

All the tests have been simulated with the computer model. The computer generated values are given in Appendices B, C, D, E, F and G. The computer generated reduction of magnetic field in percent are summarized in Table 5.6, columns 2 and 4 for the 25 Ampere and 50 Ampere levels respectively.

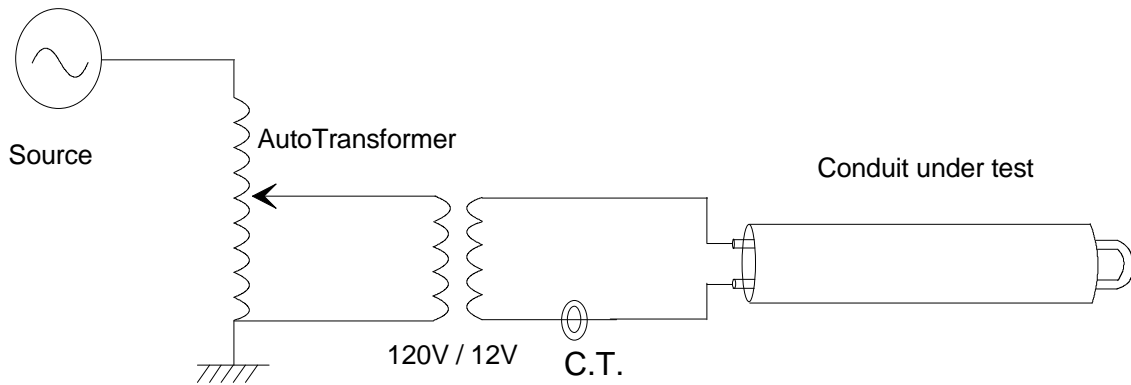


Figure 5.1. Laboratory Setup for EMF Measurements at 60 Hz (Power Frequency)

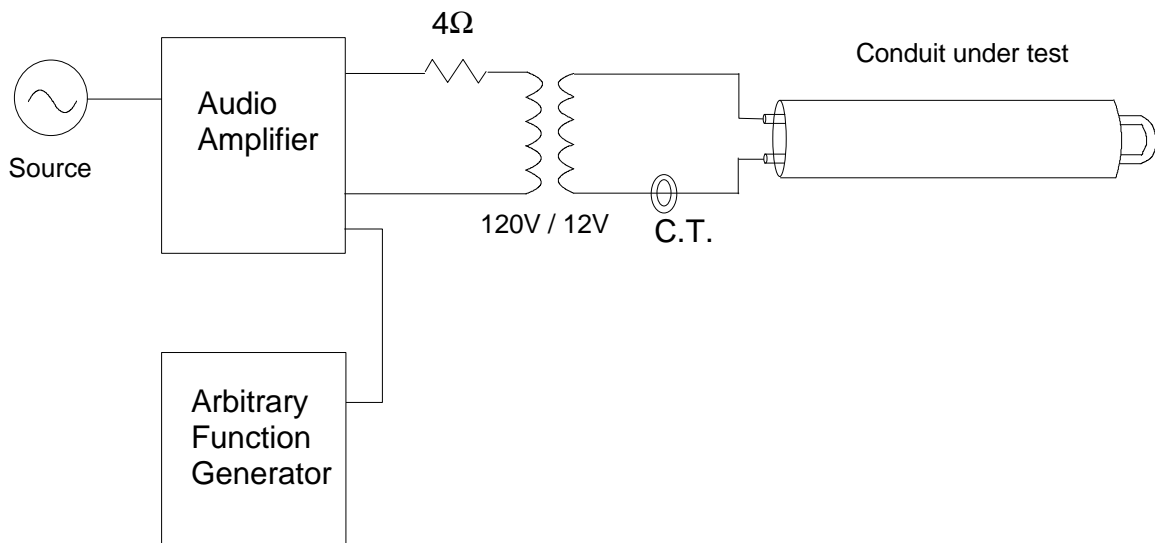


Figure 5.2 Laboratory Setup for EMF Measurements at Harmonics

Table 5.1. List of Conduit and Conductor Samples Used for Experimental Verification

Sample No.	Sample Description
1	Aluminum Conduit, ARC, 2 inch, 3/0
2	Steel Conduit, EMT, 2 inch, 3/0
3	Steel Conduit, IMC, 2 inch, 3/0
4	Steel Conduit, GRC, 3/4 inch, #8
5	Aluminum Conduit, ARC, 3/4 inch, #8
6	Steel Conduit, GRC, 2 inch, 3/0
7	Steel Conduit, EMT, 3/4 inch, #8
8	Steel Conduit, IMC, 3/4 inch, #8
9	Flexible Steel Conduit, 3/4 inch, #8
10	Steel Conduit, IMC 1 1/2 inch, 3/0
11	Steel Conduit, EMT, 1 inch, #6
12	Steel Conduit, IMC, 3/4 inch, #8
13	Steel Conduit, EMT, 1/2 inch, #10
14	Steel Conduit, EMT, 1/2 inch, #10
15	Steel Conduit, IMC, 3/4 inch, #8
16	Steel Conduit, EMT, 1 inch, #6
17	Steel Conduit, IMC, 1 1/2 inch, 3/0

**Table 5.2. Magnetic Field Measurements in mGauss. Near
Conduit-Encased Circuit, 25 Amperes, 60 Hz**

Sample No.	Description	Point 1 a+6.5cm (max/min)	Point 2 a+11.5cm (max/min)	Point 3 a+16.5cm (max/min)	Point 4 a+21.5cm (max/min)
1	Aluminum Conduit, ARC, 2 inch, 3/0	128.3/59.8	50.8/28.3	25.1/16.0	15.4/10.5
2	Steel Conduit, EMT, 2 inch, 3/0	27.5/18.6	10.4/8.6	5.63/4.7	3.98/3.1
3	Steel Conduit, IMC, 2 inch, 3/0	17.6/11.4	7.08/5.63	4.23/3.43	3.08/1.56
4	Steel Conduit, GRC, 3/4 inch, #8	4.98/4.13	2.14/1.23	1.54/0.93	1.38/0.91
5	Aluminum Conduit, ARC, 3/4 inch, #8	60.5/43.8	21.5/14.7	10.5/8.75	5.7/5.03
6	Steel Conduit, GRC, 2 inch, 3/0	12.5/8.5	5.53/3.65	3.03/1.72	1.65/1.19
7	Steel Conduit, EMT, 3/4 inch, #8	5.85/5.13	2.78/2.05	1.43/1.29	1.3/0.88
8	Steel Conduit, IMC, 3/4 inch, #8	6.23/3.9	2.85/1.23	1.65/0.84	1.40/0.81
9	Flexible Steel Conduit, 3/4 inch, #8	11.1/8.4	4.1/3.5	2.5/1.51	1.54/1.32
10	Steel Conduit, IMC 1 1/2 inch, 3/0	17.2/15	7.73/6.68	4.18/3.55	2.7/2.18
11	Steel Conduit, EMT, 1 inch, #6	7.28/6.03	3.2/1.39	1.69/1.07	1.39/1.01
12	Steel Conduit, IMC, 3/4 inch, #8	6.18/5.25	2.8/1.76	1.66/1.18	1.42/1.02
13	Steel Conduit, EMT, 1/2 inch, #10	6.58/4.65	1.73/1.20	1.33/1.03	1.19/0.93
14	Steel Conduit, EMT, 1/2 inch, #10	6.53/3.98	1.93/1.26	1.35/0.86	1.18/0.83
15	Steel Conduit, IMC, 3/4 inch, #8	5.5/4.55	2.37/1.78	1.49/1.3	1.36/1.15
16	Steel Conduit, EMT, 1 inch, #6	8.15/7.4	3.45/3.05	1.73/1.45	1.28/1.21
17	Steel Conduit, IMC, 1 1/2 inch, 3/0	15.9/13.5	7.05/4	3.45/2.25	3/1.398

a is the outside radius of the conduit under test

Table 5.3. Magnetic Field Measurements in mGauss Near Aerial Circuit, 25 Amperes, 60 Hz

Sample No.	Description	Point 1	Point 2	Point 3	Point 4
		a+6.5cm (max/min)	a+11.5cm (max/min)	a+16.5cm (max/min)	a+21.5cm (max/min)
1	Two Wire, 1/2 inch, #10	48.5/32.3	12.2/9.28	6.75/5.13	4.18/3.9
2	Two Wire, 3/4 inch, #8	40.5/28	18.6/16.5	10.3/8.78	6.05/4.95
3	Two Wire, 1 inch, #6	50/34.75	19.3/13.8	6.65/5.85	4.1/3.575
4	Two Wire, 1 1/2 inch, 3/0	117/91.5	50.5/37	23/19.28	14.9/10.7
5	Two Wire, 2 inch, 3/0	114/74.8	45.5/37.8	23.3/18.8	13.1/12.1

a is the outside radius of the conduit under test

**Table 5.4 Magnetic Field Measurements in mGauss Near
Conduit-Encased Circuit, 50 Amperes, 60 Hz**

Sample No.	Description	Point 1 a+6.5cm (max/min)	Point 2 a+11.5cm (max/min)	Point 3 a+16.5cm (max/min)	Point 4 a+21.5cm (max/min)
1	Aluminum Conduit, ARC, 2 inch, 3/0	248/113	97.3/58.5	45.5/30.8	29.5/18.8
2	Steel Conduit, EMT, 2 inch, 3/0	45.8/34.5	17/14.28	8.95/7.75	6/5.15
3	Steel Conduit, IMC, 2 inch, 3/0	34.5/22	12.8/10.1	6.88/5.15	4.95/3.45
4	Steel Conduit, GRC, 3/4 inch, #8	9.18/7.28	4.3/1.85	2.95/0.99	1.85/1.08
5	Aluminum Conduit, ARC, 3/4 inch, #8	96.8/83.3	36.8/31.0	17.7/16.4	11.2/8.35
6	Steel Conduit, GRC, 2 inch, 3/0	22/14.5	9.35/7.03	4.88/3.65	3.25/2.35
7	Steel Conduit, EMT, 3/4 inch, #8	13.9/11.2	4.7/4.23	2.9/2.2	2.18/1.31
8	Steel Conduit, IMC, 3/4 inch, #8	10.4/6.65	4.55/1.64	2.88/1.07	1.84/0.88
9	Flexible Steel Conduit, 3/4 inch, #8	17.8/14.2	6.23/5.55	3.5/3.0	2.65/1.73
10	Steel Conduit, IMC 1 1/2 inch, 3/0	33.25/28	14.1/11.9	6.88/6.35	4.25/3.98
11	Steel Conduit, EMT, 1 inch, #6	11.83/10	5.25/2.5	2.98/1.34	1.93/1.27
12	Steel Conduit, IMC, 3/4 inch, #8	10.8/8.9	4.6/3.03	2.95/1.34	1.96/1.09
13	Steel Conduit, EMT, 1/2 inch, #10	10.7/9.83	3.18/2.02	1.68/1.40	1.48/1.17
14	Steel Conduit, EMT, 1/2 inch, #10	13.0/8.33	3.98/1.43	1.88/1.13	1.47/0.99
15	Steel Conduit, IMC, 3/4 inch, #8	8.78/7.35	3.6/2.98	1.93/1.67	1.61/1.27
16	Steel Conduit, EMT, 1 inch, #6	15.6/11.8	6.28/4.03	3.15/2.15	1.848/1.5
17	Steel Conduit, IMC, 1 1/2 inch, 3/0	28.75/25	10.85/8.6	6.55/4.68	4.75/2.85

a is the outside radius of the conduit under test

Table 5.5. Magnetic Field Measurements in mGauss Near Aerial Circuit, 50 Amperes, 60 Hz

Sample No.	Description	Point 1	Point 2	Point 3	Point 4
		a+6.5cm (max/min)	a+11.5cm (max/min)	a+16.5cm (max/min)	a+21.5cm (max/min)
1	Two Wire, 1/2 inch, #10	110/72.3	24.3/17.9	11.8/9.75	8.48/6.8
2	Two Wire, 3/4 inch, #8	101/83.5	39.0/32.0	19.0/16.5	11.4/9.5
3	Two Wire, 1 inch, #6	98.3/76.5	34.8/30.8	14.5/11.8	8.18/6.28
4	Two Wire, 1 1/2 inch, 3/0	250/178	98.5/75.8	53.5/39.3	31.3/22.3
5	Two Wire, 2 inch, 3/0	236/139	90/72	43/38.5	27/24

a is the outside radius of the conduit under test

Table 5.6. Measured and Computed Reduction of Magnetic Field in Percent. Conduit-Encased Circuit, 60 Hz

Sample No.	Description	Measured (25Amps) (max/min)	Computed (25Amps) (max/min)	Measured (50Amps) (max/min)	Computed (50Amps) (max/min)
1	Aluminum Conduit, ARC, 2 inch, 3/0	18.3/0.0	4.1/3.9	19.8/0.0	5.1/4.2
2	Steel Conduit, EMT, 2 inch, 3/0	75.4/74.6	90.0/89.6	79.7/78.4	89.1/88.5
3	Steel Conduit, IMC, 2 inch, 3/0	84.7/81.8	94.5/94.0	85.6/84.2	93.9/93.3
4	Steel Conduit, GRC, 3/4 inch, #8	87.2/84.6	91.8/91.7	92.0/87.0	90.9/90.7
5	Aluminum Conduit, ARC, 3/4 inch, #8	8.0/0.0	1.4/1.36	4.6/4.0	1.42/1.28
6	Steel Conduit, GRC, 2 inch, 3/0	90.0/87.8	96.0/95.9	90.1/89.2	95.6/95.4
7	Steel Conduit, EMT, 3/4 inch, #8	84.2/83.8	82.9/82.8	86.6/85.0	81.2/81.16
8	Steel Conduit, IMC, 3/4 inch, #8	88.2/82.5	89.7/89.5	92.8/86.7	88.7/88.4
9	Flexible Steel Conduit, 3/4 inch, #8	76.2/75.2	n/a	82.3/81.2	n/a
10	Steel Conduit, IMC 1 1/2 inch, 3/0	83.4/81.7	93.5/93.1	86.5/83.6	92.5/92.0
11	Steel Conduit, EMT, 1 inch, #6	81.5/77.4	85.8/85.7	86.8/82.2	84.7/84.5
12	Steel Conduit, IMC, 3/4 inch, #8	84.1/82.5	same as case 8	90.1/86.2	same as case 8
13	Steel Conduit, EMT, 1/2 inch, #10	82.2/81.0	79.31/79.3	86.4/85.9	76.32/76.3
14	Steel Conduit, EMT, 1/2 inch, #10	84.0/80.6	same as case 13	88.6/84.6	same as case 13
15	Steel Conduit, IMC, 3/4 inch, #8	84.2/83.7	same as case 8	89.6/89.4	same as case 8
16	Steel Conduit, EMT, 1 inch, #6	77.1/74.5	same as case 11	82.3/80.4	same as case 11
17	Steel Conduit, IMC, 1 1/2 inch, 3/0	87.4/84.3	same as case 10	87.5/87.5	same as case 10

Table 5.7. Magnetic Field Measurements in mGauss Near Conduit-Encased Circuit, 25 Amperes, 190 Hz - Near 3rd Harmonic

Sample No.	Description	Point 1 a+6.5cm (max/min)	Point 2 a+11.5cm (max/min)	Point 3 a+16.5cm (max/min)	Point 4 a+21.5cm (max/min)
1	Aluminum Conduit, ARC, 2 inch, 3/0	74/24.75	27/13.43	12.15/7.3	7.78/5.43
2	Steel Conduit, EMT, 2 inch, 3/0	19.3/14.2	8.18/6.83	4.75/4.03	3.63/3.13
3	Steel Conduit, IMC, 2 inch, 3/0	11.6/7.65	5.68/4.38	3.58/2.95	3.1/2.45
4	Steel Conduit, GRC, 3/4 inch, #8	4.4/4.05	3.29/2.95	3.35/2.65	3.25/2.56
5	Aluminum Conduit, ARC, 3/4 inch, #8	50.5/38.3	14.4/10.8	10.0/7.55	6.05/5.0
6	Steel Conduit, GRC, 2 inch, 3/0	5.8/4.25	3.3/2.85	2.89/2.28	2.78/1.52
7	Steel Conduit, EMT, 3/4 inch, #8	7.28/6.08	3.53/3.13	3.05/2.58	3.05/2.3
8	Steel Conduit, IMC, 3/4 inch, #8	5.28/4.1	3.15/2.78	3.0/2.48	3.0/1.93
9	Flexible Steel Conduit, 3/4 inch, #8	11.8/9.3	4.78/3.8	3.7/2.9	3.3/2.55
10	Steel Conduit, IMC 1 1/2 inch, 3/0	12.1/10.4	5.3/4.95	3.48/3.08	2.9/2.23
11	Steel Conduit, EMT, 1 inch, #6	6.8/5.9	3.25/2.83	2.9/1.848	2.95/1.74
12	Steel Conduit, IMC, 3/4 inch, #8	5.75/4.48	3.43/3.0	3.14/2.74	3.18/2.5
13	Steel Conduit, EMT, 1/2 inch, #10	6.15/4.53	3.15/2.8	3.0/2.44	3.02/2.35
14	Steel Conduit, EMT, 1/2 inch, #10	6.8/4.1	3.08/2.65	3.0/2.35	3.0/2.1
15	Steel Conduit, IMC, 3/4 inch, #8	5.25/4.4	3.18/2.75	3.0/2.4	3.0/2.15
16	Steel Conduit, EMT, 1 inch, #6	7.15/6.63	3.5/2.95	2.9/1.633	2.8/1.708
17	Steel Conduit, IMC, 1 1/2 inch, 3/0	10.33/9.6	4.75/4.4	3.28/2.98	2.875/2.3

a is the outside radius of the conduit under test

Table 5.8. Magnetic Field Measurements in mGauss Near Aerial Circuit, 25 Amperes, 190 Hz - Near 3rd Harmonic

Sample No.	Description	Point 1 a+6.5cm (max/min)	Point 2 a+11.5cm (max/min)	Point 3 a+16.5cm (max/min)	Point 4 a+21.5cm (max/min)
1	Two Wire, 1/2 inch, #10	58/36.8	11.8/10.0	7.15/6.1	6.03/4.13
2	Two Wire, 3/4 inch, #8	54.5/46.3	19.2/17.0	10.5/9.28	6.25/5.9
3	Two Wire, 1 inch, #6	56.8/43.3	19.45/15	8.35/6.98	5.13/4.35
4	Two Wire, 1 1/2 inch, 3/0	122/88.3	48.3/35.8	25.8/17.9	16.2/10.9
5	Two Wire, 2 inch, 3/0	115/72.3	42.3/36.5	21.3/18.9	12.6/12.1

a is the outside radius of the conduit under test

**Table 5.9. Magnetic Field Measurements in mGauss Near
Conduit-Encased Circuit, 50 Amperes, 190 Hz - Near 3rd Harmonic**

Sample No.	Description	Point 1 a+6.5cm (max/min)	Point 2 a+11.5cm (max/min)	Point 3 a+16.5cm (max/min)	Point 4 a+21.5cm (max/min)
1	Aluminum Conduit, ARC, 2 inch, 3/0	140/50	55/27.75	26/15.2	15/10.63
2	Steel Conduit, EMT, 2 inch, 3/0	34/26.13	13.7/11.4	7.8/6.75	5.95/5
3	Steel Conduit, IMC, 2 inch, 3/0	20.8/13.9	9.45/7.28	6.03/4.68	5.05/3.85
4	Steel Conduit, GRC, 3/4 inch, #8	7.53/6.63	5.5/4.6	5.03/4.3	5.05/3.9
5	Aluminum Conduit, ARC, 3/4 inch, #8	108/79.3	39.0/27.0	17.8/13.5	10.8/8.35
6	Steel Conduit, GRC, 2 inch, 3/0	9.93/7.35	5.35/4.65	4.43/3.73	4.3/3.2
7	Steel Conduit, EMT, 3/4 inch, #8	12.9/10.6	5.68/5.25	4.95/3.9	4.8/3.65
8	Steel Conduit, IMC, 3/4 inch, #8	7.9/7.28	4.8/4.18	4.2/3.7	4.28/3.25
9	Flexible Steel Conduit, 3/4 inch, #8	20.2/16.1	7.83/5.75	5.68/4.1	5.05/3.73
10	Steel Conduit, IMC 1 1/2 inch, 3/0	21/17.38	9.2/8.05	5.675/5.4	4.83/3.95
11	Steel Conduit, EMT, 1 inch, #6	13.5/10.7	6.15/4.7	4.7/3.525	4.25/3.23
12	Steel Conduit, IMC, 3/4 inch, #8	9.18/3.88	5.1/4.5	4.65/3.9	4.7/3.5
13	Steel Conduit, EMT, 1/2 inch, #10	8.53/7.1	4.73/4.05	4.35/3.68	4.6/3.35
14	Steel Conduit, EMT, 1/2 inch, #10	10.6/6.18	4.63/3.9	4.25/3.5	4.25/3.25
15	Steel Conduit, IMC, 3/4 inch, #8	8.68/7.35	4.95/4.15	4.55/3.8	4.48/3.35
16	Steel Conduit, EMT, 1 inch, #6	13.2/11	5.95/4.95	4.53/3.73	4.3/3.25
17	Steel Conduit, IMC, 1 1/2 inch, 3/0	17.7/16.1	7.95/7.5	5.45/4.88	4.7/3.9

a is the outside radius of the conduit under test

Table 5.10. Magnetic Field Measurements in mGauss Near Aerial Circuit, 50 Amperes, 190 Hz - Near 3rd Harmonic

Sample No.	Description	Point 1 a+6.5cm (max/min)	Point 2 a+11.5cm (max/min)	Point 3 a+16.5cm (max/min)	Point 4 a+21.5cm (max/min)
1	Two Wire, 1/2 inch, #10	101/77.0	25.3/18.6	13.3/11.9	9.25/7.58
2	Two Wire, 3/4 inch, #8	108/92	41.0/35.0	19.6/17.8	11.3/10.6
3	Two Wire, 1 inch, #6	105/63.8	38.5/28.5	15.3/14.3	8.98/7.58
4	Two Wire, 1 1/2 inch, 3/0	230/180	97.8/78.5	52.8/38.8	31/22.75
5	Two Wire, 2 inch, 3/0	219/150	97/74	42/39.5	27.25/26

a is the outside radius of the conduit under test

**Table 5.11. Measured and Computed Reduction of Magnetic Field
in Percent. Conduit-Encased Circuit, 190 Hz**

Sample No.	Description	Measured (25Amps) (max/min)	Computed (25Amps) (max/min)	Measured (50Amps) (max/min)	Computed (50Amps) (max/min)
1	Aluminum Conduit, ARC, 2 inch, 3/0	31.4/18.3	31.8/26.1	32.4/20.6	31.7/26.2
2	Steel Conduit, EMT, 2 inch, 3/0	78.6/78.2	96.19/96.17	82.7/82.5	95.6/95.5
3	Steel Conduit, IMC, 2 inch, 3/0	85.4/83.8	97.3/96.8	88.6/87.0	96.8/96.5
4	Steel Conduit, GRC, 3/4 inch, #8	75.5/72.7	96.3/96.2	79.7/77.3	95.5/95.4
5	Aluminum Conduit, ARC, 3/4 inch, #8	21.9/10.1	12.4/11.3	20.5/4.6	12.7/11.4
6	Steel Conduit, GRC, 2 inch, 3/0	90.4/87.9	97.3/96.6	91.8/90.9	97.0/96.5
7	Steel Conduit, EMT, 3/4 inch, #8	75.4/72.6	91.3/91.2	79.3/76.6	90.0/89.9
8	Steel Conduit, IMC, 3/4 inch, #8	78.8/74.3	95.3/95.2	82.2/80.4	94.5/94.3
9	Flexible Steel Conduit, 3/4 inch, #8	70.8/66.4	n/a	77.0/72.1	n/a
10	Steel Conduit, IMC 1 1/2 inch, 3/0	86.9/84.2	97.1/96.9	88.8/87.2	96.43/96.42
11	Steel Conduit, EMT, 1 inch, #6	75.3/69.8	93.6/93.4	74.9/73.3	92.6/92.4
12	Steel Conduit, IMC, 3/4 inch, #8	75.4/72.7	same as case 8	82.0/78.4	same as case 8
13	Steel Conduit, EMT, 1/2 inch, #10	67.7/65.7	88.6/88.5	73.5/72.6	86.49/86.46
14	Steel Conduit, EMT, 1/2 inch, #10	68.2/67.6	same as case 13	74.7/73.3	same as case 13
15	Steel Conduit, IMC, 3/4 inch, #8	78.0/74.3	same as case 8	81.8/79.3	same as case 8
16	Steel Conduit, EMT, 1 inch, #6	75.6/70.0	same as case 11	84.1/73.6	same as case 11
17	Steel Conduit, IMC, 1 1/2 inch, 3/0	87.8/84.8	same as case 10	89.7/87.9	same as case 10

Table 5.13. Magnetic Field Measurements in mGauss Near Conduit-Encased Circuit, 25 Amperes, 310 Hz - Near 5rd Harmonic

Sample No.	Description	Point 1 a+6.5cm (max/min)	Point 2 a+11.5cm (max/min)	Point 3 a+16.5cm (max/min)	Point 4 a+21.5cm (max/min)
1	Aluminum Conduit, ARC, 2 inch, 3/0	52.3/13.4	17.2/8.08	5.45/4.83	4.83/3.18
2	Steel Conduit, EMT, 2 inch, 3/0	14.6/10.3	6.2/5	3.8/3.225	3.2/2.725
3	Steel Conduit, IMC, 2 inch, 3/0	7.48/5.15	3.95/3.1	3.08/2.48	2.98/2.2
4	Steel Conduit, GRC, 3/4 inch, #8	3.73/3.4	3.06/2.85	3.1/2.6	3.2/2.68
5	Aluminum Conduit, ARC, 3/4 inch, #8	45.0/33.0	14.1/9.85	6.43/4.8	5.05/3.0
6	Steel Conduit, GRC, 2 inch, 3/0	3.63/2.93	2.89/1.86	2.84/1.71	2.69/1.61
7	Steel Conduit, EMT, 3/4 inch, #8	6.28/5.73	3.6/3.04	3.13/2.7	3.05/2.5
8	Steel Conduit, IMC, 3/4 inch, #8	4.28/3.73	3.0/2.65	2.95/2.4	3.0/1.86
9	Flexible Steel Conduit, 3/4 inch, #8	11.4/9.58	4.88/3.75	3.65/2.8	3.25/2.45
10	Steel Conduit, IMC 1 1/2 inch, 3/0	7.98/6.78	3.93/3.38	3.1/2.625	2.83/1.78
11	Steel Conduit, EMT, 1 inch, #6	7.28/5.53	3.35/2.88	2.93/1.82	2.83/1.73
12	Steel Conduit, IMC, 3/4 inch, #8	4.75/3.0	3.1/2.83	3.03/2.6	3.0/1.91
13	Steel Conduit, EMT, 1/2 inch, #10	5.35/4.9	3.04/2.75	3.01/2.45	3.02/2.24
14	Steel Conduit, EMT, 1/2 inch, #10	6.78/3.7	2.98/2.5	2.95/1.82	2.95/1.78
15	Steel Conduit, IMC, 3/4 inch, #8	4.2/3.68	3.05/2.75	3.0/2.43	3.0/2.25
16	Steel Conduit, EMT, 1 inch, #6	6.75/5.68	3.35/2.9	2.85/2.25	2.78/1.72
17	Steel Conduit, IMC, 1 1/2 inch, 3/0	7.08/6.25	3.65/3.28	2.93/2.58	2.83/2.15

a is the outside radius of the conduit under test

Table 5.14. Magnetic Field Measurements in mGauss Near Aerial Circuit, 25 Amperes, 310 Hz - Near 5rd Harmonic

Sample No.	Description	Point 1 a+6.5cm (max/min)	Point 2 a+11.5cm (max/min)	Point 3 a+16.5cm (max/min)	Point 4 a+21.5cm (max/min)
1	Two Wire, 1/2 inch, #10	48.3/37.5	12.3/9.9	7.35/5.75	5.45/4.25
2	Two Wire, 3/4 inch, #8	56.3/47.0	18.6/16.4	10.1/9.0	6.0/5.5
3	Two Wire, 1 inch, #6	72.3/34.3	17.7/13.8	8.1/6.725	5.08/3.75
4	Two Wire, 1 1/2 inch, 3/0	114/83.8	47.5/36.3	25.5/16.9	13/10.05
5	Two Wire, 2 inch, 3/0	113/75.3	45.8/36.8	21.8/12	12.85/12

a is the outside radius of the conduit under test

**Table 5.15. Magnetic Field Measurements in mGauss Near
Conduit-Encased Circuit, 50 Amperes, 310 Hz - Near 5rd Harmonic**

Sample No.	Description	Point 1 a+6.5cm (max/min)	Point 2 a+11.5cm (max/min)	Point 3 a+16.5cm (max/min)	Point 4 a+21.5cm (max/min)
1	Aluminum Conduit, ARC, 2 inch, 3/0	96.8/30.5	39/15.88	15.05/9.4	10.55/6.5
2	Steel Conduit, EMT, 2 inch, 3/0	27.8/17.5	10.2/8.55	6.18/5.25	5.13/4.23
3	Steel Conduit, IMC, 2 inch, 3/0	12.7/9.03	6.55/5.15	4.98/3.93	4.6/3.375
4	Steel Conduit, GRC, 3/4 inch, #8	5.9/5.53	4.85/4.08	4.86/3.91	4.05/3.85
5	Aluminum Conduit, ARC, 3/4 inch, #8	91.5/63.0	27.0/18.5	14.4/9.9	8.98/6.4
6	Steel Conduit, GRC, 2 inch, 3/0	5.78/4.75	4.3/3.7	4.05/3.19	4.07/3.1
7	Steel Conduit, EMT, 3/4 inch, #8	10.3/9.38	5.33/4.95	4.78/3.95	4.65/3.58
8	Steel Conduit, IMC, 3/4 inch, #8	6.43/5.5	4.65/4.05	4.28/3.65	4.25/3.23
9	Flexible Steel Conduit, 3/4 inch, #8	18.9/13.2	7.83/5.9	5.63/4.2	5.05/3.8
10	Steel Conduit, IMC 1 1/2 inch, 3/0	13.1/11.3	6.43/5.45	4.95/3.98	4.35/3.35
11	Steel Conduit, EMT, 1 inch, #6	10.3/8.65	5.03/4.73	4.28/3.73	4.2/3.225
12	Steel Conduit, IMC, 3/4 inch, #8	7.55/6.2	4.8/4.05	4.45/3.65	4.55/3.45
13	Steel Conduit, EMT, 1/2 inch, #10	8.1/7.25	4.68/3.93	4.38/3.58	4.75/3.28
14	Steel Conduit, EMT, 1/2 inch, #10	10.6/4.88	4.03/3.35	3.8/3.01	4.25/3.18
15	Steel Conduit, IMC, 3/4 inch, #8	6.98/6.0	4.8/4.0	4.55/3.65	4.65/3.35
16	Steel Conduit, EMT, 1 inch, #6	9.65/9.23	5.33/4.65	4.35/3.68	4.18/3.18
17	Steel Conduit, IMC, 1 1/2 inch, 3/0	11.7/10.5	5.9/5.45	4.625/4	4.28/3.45

a is the outside radius of the conduit under test

Table 5.16. Magnetic Field Measurements in mGauss Near Aerial Circuit, 50 Amperes, 310 Hz - Near 5rd Harmonic

Sample No.	Description	Point 1 a+6.5cm (max/min)	Point 2 a+11.5cm (max/min)	Point 3 a+16.5cm (max/min)	Point 4 a+21.5cm (max/min)
1	Two Wire, 1/2 inch, #10	94.8/67.5	25.0/17.7	11.8/9.88	9.1/7.13
2	Two Wire, 3/4 inch, #8	109/93.3	40.0/34.5	18.8/17.5	10.8/10.2
3	Two Wire, 1 inch, #6	119/82.5	41.8/26.5	14.48/13	8.78/7.58
4	Two Wire, 1 1/2 inch, 3/0	210/182	97/74	51/38.5	30.3/22.3
5	Two Wire, 2 inch, 3/0	208/152	96.5/75.5	44.3/38.8	26.5/23

a is the outside radius of the conduit under test

**Table 5.17. Measured and Computed Reduction of Magnetic Field
in Percent. Conduit-Encased Circuit, 310 Hz**

Sample No.	Description	Measured (25Amps) (max/min)	Computed (25Amps) (max/min)	Measured (50Amps) (max/min)	Computed (50Amps) (max/min)
1	Aluminum Conduit, ARC, 2 inch, 3/0	73.4/63.4	51.1/42.5	76.6/59.8	51.2/42.5
2	Steel Conduit, EMT, 2 inch, 3/0	82.8/80.8	97.2/96.8	86.3/85.7	96.6/96.4
3	Steel Conduit, IMC, 2 inch, 3/0	86.9/86.4	97.2/96.5	90.6/89.6	96.4/89.4
4	Steel Conduit, GRC, 3/4 inch, #8	74.4/73.2	97.0/96.8	80.5/79.8	96.3/96.1
5	Aluminum Conduit, ARC, 3/4 inch, #8	40.5/24.1	26.0/23.6	39.9/22.2	26.4/23.7
6	Steel Conduit, GRC, 2 inch, 3/0	90.8/89.1	97.0/96.3	92.6/92.1	96.7/96.1
7	Steel Conduit, EMT, 3/4 inch, #8	73.5/71.9	94.0/93.9	79.5/77.2	92.9/92.7
8	Steel Conduit, IMC, 3/4 inch, #8	78.9/74.3	96.5/96.4	82.5/80.1	95.8/95.6
9	Flexible Steel Conduit, 3/4 inch, #8	70.3/65.8	n/a	76.9/71.6	n/a
10	Steel Conduit, IMC 1 1/2 inch, 3/0	87.7/87.3	97.1/96.9	90.8/90.3	96.6/96.5
11	Steel Conduit, EMT, 1 inch, #6	72.4/69.8	95.6/95.5	75.5/75.1	94.7/94.6
12	Steel Conduit, IMC, 3/4 inch, #8	78.2/73.7	same as case 8	81.7/78.8	same as case 8
13	Steel Conduit, EMT, 1/2 inch, #10	67.0/66.0	91.6/91.5	71.2/70.9	89.85/89.78
14	Steel Conduit, EMT, 1/2 inch, #10	72.8/66.9	same as case 13	74.7/73.4	same as case 13
15	Steel Conduit, IMC, 3/4 inch, #8	76.9/74.1	same as case 8	82.1/78.6	same as case 8
16	Steel Conduit, EMT, 1 inch, #6	70.8/70.5	same as case 11	75.4/75.3	same as case 11
17	Steel Conduit, IMC, 1 1/2 inch, 3/0	88.2/86.7	same as case 10	91.3/90.2	same as case 10

6.0 Factors Affecting Magnetic Fields

In this section, we present examples which illustrate the major factors affecting electromagnetic fields. It has been verified that steel conduit is very effective in shielding magnetic fields. The shielding effectiveness is maximum when the system is installed in such a way as to minimize current flow in ground conductors under normal operating conditions. Proper grounding and bonding techniques, in accordance with the National Electrical Code will achieve this. In this section we examine the effects of ground currents in a multiple grounded system. For this purpose we consider a rather simple system which is illustrated in Figure 6.1. It consists of a power company system which feeds a secondary distribution system in a GRC steel conduit. The system supplies an unbalanced load.

Figure 6.2 illustrates the electric current flow in the conductors and steel conduit for the case of a ground impedance of 200 ohms at the end of the conduit. For this condition, the magnetic field density near the conduit is illustrated in Figure 6.3.

Now consider the same case but with a ground impedance of 0.5 ohms (extreme case) at the end of the conduit. The flow of current in the conductors and the conduit is illustrated in Figure 6.4. Note that some of the current returns through the soil. For this case, the magnetic field density is illustrated in Figure 6.5. Note that the field in this case is higher than in the previous case, even if the load of the system remains the same.

NET - Network System Editor V 1.00
Case: Example: Effects of unbalance on
Date: 02/09/97
Time: 15:53:46.54

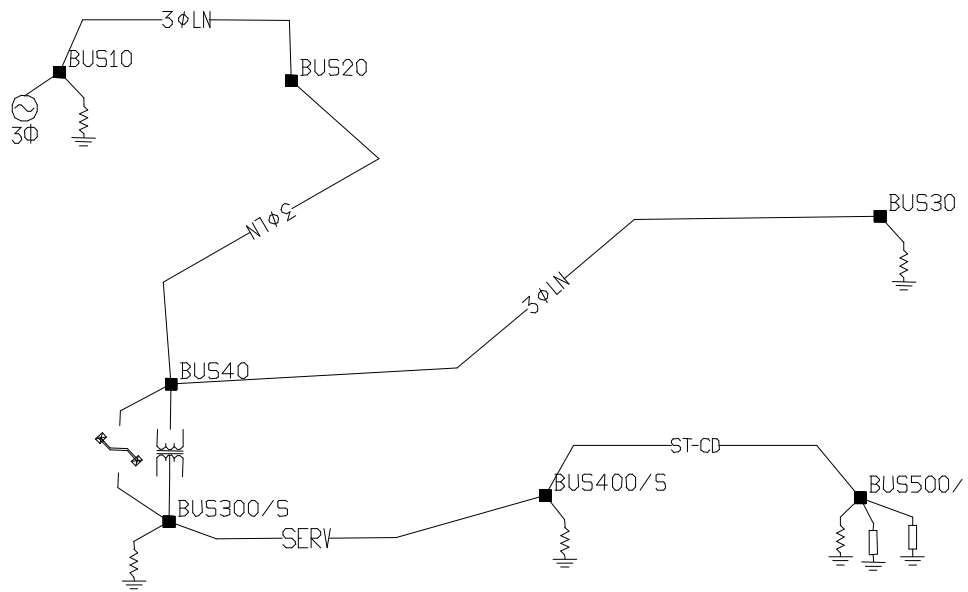


Figure 6.1. Example System for Studying Magnetic Fields in Actual Systems

Report Device Volt/Currents		F1 Return		
Device Number: 12 Device Title: 150 Feet of GRC, 1-1/2inch, A 1/0, Copper #1 Model Has Been Computed at Frequency: 60.00 Hertz				
Node Name	Voltage		Electric Current	
	Magnitude (Volts)	Phase (Degrees)	Magnitude (Amperes)	Phase (Degrees)
BUS400_L1	118.09	-2.19	80.89	-13.80
BUS400_L2	117.53	178.16	41.87	167.16
BUS400_NN	1.21	16.50	28.67	176.10
BUS400_NN	1.21	16.50	12.16	138.56
BUS500_L1	116.33	-2.04	80.89	166.20
BUS500_L2	116.11	178.04	41.87	-12.84
BUS500_NN	2.30	21.00	28.67	-3.90
BUS500_NN	2.30	21.00	12.16	-41.44
F2 More ...				
Program: SCA Vs2.0		Form Name: REP_DVIO		Print [Alt P] Save [Alt S]

Figure 6.2. Flow of Electric Current in Conductors and Conduit for a 200 Ohm Ground Resistance at End of Circuit

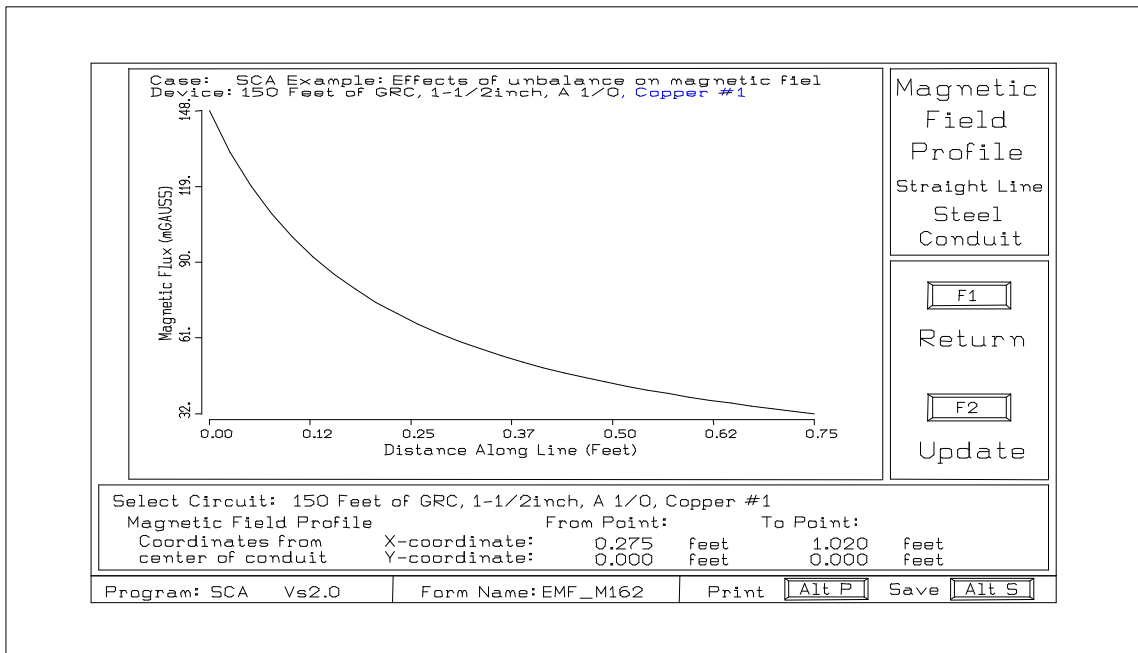


Figure 6.3. Computed Magnetic Field Density Near the Conduit for the Condition of Figure 6.2

Report Device Volt/Currents				
Device Number: 12				
Device Title: 150 Feet of GRC, 1-1/2inch, A 1/0, Copper #1				
Model Has Been Computed at Frequency: 60.00 Hertz				
Node Name	Voltage		Electric Current	
	Magnitude (Volts)	Phase (Degrees)	Magnitude (Amperes)	Phase (Degrees)
BUS400_L1	116.97	-2.58	80.93	-13.78
BUS400_L2	118.68	178.55	41.85	167.15
BUS400_NN	0.42	-91.76	26.73	173.84
BUS400_NN	0.42	-91.76	11.76	143.20
BUS500_L1	115.17	-2.46	80.93	166.22
BUS500_L2	117.29	178.46	41.85	-12.85
BUS500_NN	0.90	-1.63	26.73	-6.16
BUS500_NN	0.90	-1.63	11.76	-36.80

More ...

Program: SCA Vs2.0 Form Name: REP_DVIO Print [Alt P] Save [Alt S]

Figure 6.4. Flow of Electric Current in Conductors and Conduit for a 0.5 Ohm Ground Resistance at End of Circuit

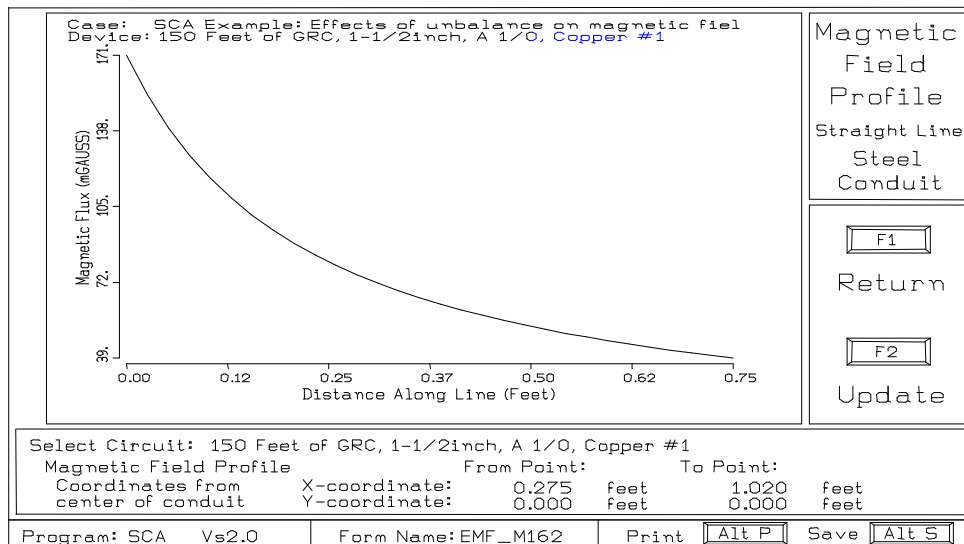


Figure 6.5. Computed Magnetic Field Density Near the Conduit for the Condition of Figure 6.4

7.0 Conclusions

The investigation consisted of laboratory tests, and the development and validation of an analytical model. Studies were performed of factors affecting electromagnetic field intensity near power circuits. The conclusions of the investigation are:

1. PVC conduit does not reduce the electromagnetic fields from encased power circuits.
2. Aluminum conduit is *practically ineffective* in reducing electromagnetic fields at power frequency (60 Hz). Magnetic field reduction in aluminum conduit encased power systems is on the order of 10%. At higher frequencies the effectiveness of aluminum to shield against electromagnetic fields increases.
3. Steel conduit is *very effective* in reducing electromagnetic fields at power frequency (60 Hz). Magnetic field reduction in steel conduit encased power systems is on the order of 70% to 95%. PVC coated steel conduit provides the same amount of reduction.
4. None of the conduit provides shielding against the contribution to electromagnetic fields from ground currents.

Appendix A: Difference Equations at Boundary Points

This appendix presents the difference equations for points at the boundary of two regions.

Assume the boundary S between region 1 and region 2 as shown in Figure A.1. The scalar magnetic potential Φ is expanded into Taylor series (around point 0) in region 1 as follows:

$$\Phi_2 \cong \Phi_0 - \frac{\partial\Phi_I}{\partial r}\Big|_0 \Delta r_1 + \frac{\partial^2\Phi_I}{\partial r^2}\Big|_0 \frac{\Delta r_1^2}{2} \quad (\text{A1})$$

$$\Phi_3 \cong \Phi_0 + \frac{\partial\Phi_I}{\partial\phi}\Big|_0 \Delta\phi + \frac{\partial^2\Phi_I}{\partial\phi^2}\Big|_0 \frac{\Delta\phi^2}{2} \quad (\text{A2})$$

$$\Phi_4 \cong \Phi_0 - \frac{\partial\Phi_I}{\partial\phi}\Big|_0 \Delta\phi + \frac{\partial^2\Phi_I}{\partial\phi^2}\Big|_0 \frac{\Delta\phi^2}{2} \quad (\text{A3})$$

The above expansions can be rewritten in the following form:

$$\frac{\partial^2\Phi_I}{\partial r^2}\Big|_0 = \frac{2}{\Delta r_1^2} [\Phi_2 - \Phi_0 + \Delta r_1 \frac{\partial\Phi_I}{\partial r}\Big|_0] \quad (\text{A4})$$

$$\frac{1}{r_0} \frac{\partial\Phi_I}{\partial r}\Big|_0 = \frac{1}{r_0} \frac{\partial\Phi_I}{\partial r}\Big|_0 \quad (\text{A5})$$

$$\frac{1}{r_0^2} \frac{\partial^2\Phi_I}{\partial\phi^2}\Big|_0 = \frac{1}{r_0^2 \Delta\phi^2} (\Phi_3 + \Phi_4 - 2\Phi_0) \quad (\text{A6})$$

Adding equation (A4) - (A6) and using the Laplace's equation for point 0, which makes the sum of the left hand side term equal to zero, and rearranging the remaining terms (i.e. solving for the derivative of the potential with respect to r), we obtain the following equation:

$$\frac{\partial\Phi_I}{\partial r}\Big|_0 = \left(\frac{2}{\Delta r_1} + \frac{1}{r_0} \right)^{-1} \left[\frac{2}{\Delta r_1^2} (\Phi_0 - \Phi_2) - \frac{1}{r_0^2 \Delta\phi^2} (\Phi_3 + \Phi_4 - 2\Phi_0) \right] \quad (\text{A7})$$

Using exactly the same procedure but now for region 2 (points 0,1,3 and 4), the following equation is obtained:

$$\frac{\partial \Phi_{II}}{\partial r} \Big|_0 = \left(\frac{2}{\Delta r_2} + \frac{1}{r_0} \right)^{-1} \left[\frac{2}{\Delta r_2^2} (\Phi_1 - \Phi_0) - \frac{1}{r_0^2 \Delta \phi^2} (\Phi_3 + \Phi_4 - 2\Phi_0) \right] \quad (\text{A8})$$

where Φ_{II} is the scalar magnetic potential in region 2. Inserting the partial derivatives from Equations (A7) and (A8) into the boundary condition defined by Equation (9) and rearranging terms, equation (14) is derived.

Finally, the boundary condition for the artificial $r = a_B$ is derived from Equation (A7),

$$\frac{\partial \Phi_I}{\partial r} \Big|_0 = \left(\frac{2}{\Delta r} + \frac{1}{r_0} \right)^{-1} \left[\frac{2}{\Delta r^2} (\Phi_0 - \Phi_2) - \frac{1}{r_0^2 \Delta \phi^2} (\Phi_3 + \Phi_4 - 2\Phi_0) \right] \quad (\text{A9})$$

Equation (15) is obtained from application of equation (A7).

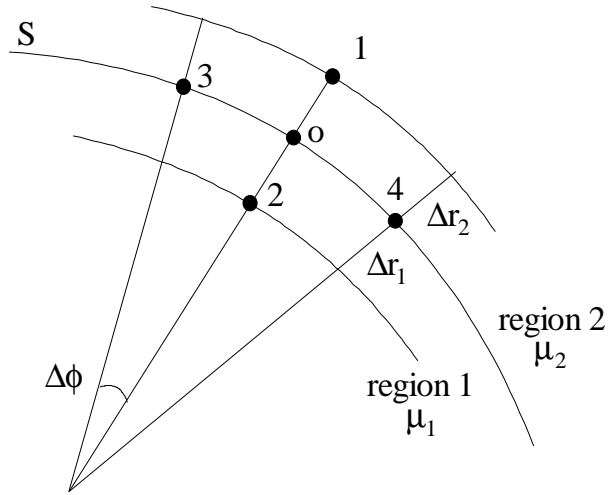


Figure A.1. Illustration of Five Neighboring Vertices

Appendix B: Computer Generated Data, 25 Amperes, 60 Hz

This appendix includes computer generated graphs of magnetic field analysis of the test systems and at locations where measurements were obtained. The current in the circuit is 25 Amperes, 60 Hz. This data has been utilized to compute the magnetic field reduction provided by steel conduit or aluminum conduit.

The data are included in Volume 2 of this report.

Appendix C: Computer Generated Data, 50 Amperes, 60 Hz

This appendix includes computer generated graphs of magnetic field analysis of the test systems and at locations where measurements were obtained. The current in the circuit is 50 Amperes, 60 Hz. This data has been utilized to compute the magnetic field reduction provided by steel conduit or aluminum conduit.

The data are included in Volume 2 of this report.

Appendix D: Computer Generated Data, 25 Amperes, 190 Hz

This appendix includes computer generated graphs of magnetic field analysis of the test systems and at locations where measurements were obtained. The current in the circuit is 25 Amperes, 190 Hz or near the 3rd harmonic. This data has been utilized to compute the magnetic field reduction provided by steel conduit or aluminum conduit.

The data are included in Volume 2 of this report.

Appendix E: Computer Generated Data, 50 Amperes, 190 Hz

This appendix includes computer generated graphs of magnetic field analysis of the test systems and at locations where measurements were obtained. The current in the circuit is 50 Amperes, 190 Hz or near the 3rd harmonic. This data has been utilized to compute the magnetic field reduction provided by steel conduit or aluminum conduit.

The data are included in Volume 2 of this report.

Appendix F: Computer Generated Data, 25 Amperes, 310 Hz

This appendix includes computer generated graphs of magnetic field analysis of the test systems and at locations where measurements were obtained. The current in the circuit is 25 Amperes, 310 Hz or near the 5th harmonic. This data has been utilized to compute the magnetic field reduction provided by steel conduit or aluminum conduit.

The data are included in Volume 2 of this report.

Appendix G: Computer Generated Data, 50 Amperes, 310 Hz

This appendix includes computer generated graphs of magnetic field analysis of the test systems and at locations where measurements were obtained. The current in the circuit is 50 Amperes, 310 Hz or near the 5th harmonic. This data has been utilized to compute the magnetic field reduction provided by steel conduit or aluminum conduit.

The data are included in Volume 2 of this report.